第27卷 第2期
2006年2月

半 导 体 学 报
CHINESE JOURNAL OF SEMICONDUCTORS

Vol.27 No.2
Feb.,2006

Quantum and Transport Mobilities of a Two-Dimensional Electron Gas in the Presence of the Rashba Spin-Orbit Interaction

Xu Wen[1,2,†]

(1 Department of Theoretical Physics, Research School of Physical Sciences and Engineering, Australian National University, Canberra ACT 0200, Australia)

(2 Institute of Solid State Physics, Chinese Academy of Sciences, Hefei 230031, China)

Abstract: A systematic theoretical approach is developed to study the electronic and transport properties of a two-dimensional electron gas (2DEG) in the presence of spin-orbit interactions induced by the Rashba effect. The standard random-phase approximation is employed to calculate the screening length caused by electron-electron interaction in different transition channels. The quantum and transport mobilities in different spin branches are evaluated using the momentum-balance equation derived from the Boltzmann equation, in which the electron interactions with both the remote and background impurities are taken into account in an InAlAs/InGaAs heterojunction at low-temperatures.

Key words: InGaAs/InAlAs HEMT; 2D modeling and simulation; polarization charges; quantum effects
PACC: 7200; 7110C
CLC number: O47 **Document code:** A **Article ID:** 0253-4177(2006)02-0204-14

1 Introduction

In recent years, the investigation of spin polarized electronic systems has become a fast-growing research field in condensed matter physics and semiconductor electronics, owing to the interesting physics behind them and to important device applications. It has been realized that spin-electronic (or spintronic) systems and devices can be realized on the basis of diluted magnetic semiconductors and narrow-gap semiconductor nanostructures. In the former case, the spin-orbit interaction (SOI) is achieved in the presence of an external magnetic field, and devices can be operated even at room-temperature. In the latter case, the SOI is introduced due to the innate features of the material systems, and a strong spin polarization can normally be achieved at relatively low-temperatures. At present, one important aspect in the field of spintronics is the study of electronic systems with a finite spin-splitting realized from narrow-gap semiconductor nanostructures in the absence of an external magnetic field. The progress made in realizing spin-split electron gas systems at zero-magnetic-field, such as InAs- and InGaAs-based two-dimensional electron gases (2DEGs)[1], has led to recent proposals dealing with advanced electronic devices such as spin-transistors[2], spin-filters[3], and spin-waveguides[4]. It is known that in narrow-gap semiconductor nanostructures such as quantum wells, the zero-magnetic-field spin splitting (or spontaneous spin splitting) of the carriers can be achieved by the inversion asymmetry of the microscopic confining potential due to the presence of the heterojunction[5]. This corresponds to an inhomogeneous surface electric field and, hence, is electrically equivalent to the Rashba spin-splitting or Rashba effect[6]. The published experimental results[7,8] have indicated that in InAs- and InGaAs-based 2DEG systems, the spontaneous spin splitting is mainly induced by the Rashba effect (with an SU(2) symmetry) which can be enhanced further with increasing the gate voltage applied. Other contributions such as the Dresselhaus term (with an SU(1,1) symmetry) are relatively weak, because they come mainly from the bulk-inversion asymmetry of the material[9]. More importantly, the strength of the Rashba spin-splitting and the corresponding SOI in

† Corresponding author. Email: wen105@rsphysse.anu.edu.au

Received 17 October 2005

©2006 Chinese Institute of Electronics

these systems can be controlled artificially by applying a gate voltage[7,8], changing the sample growth parameters[10], etc.

In order to apply spintronic systems as electronic devices such as spin-transistors, it is of fundamental importance to study the effect of SOI on the electronic and transport properties of these novel systems. At present, one of the most powerful and most popularly used experimental techniques to identify the Rashba spin splitting is magneto-transport measurement carried out in quantized magnetic fields and low-temperatures at which the Shubnikov-de Hass (SdH) oscillations are observable[1,8,10～12]. From the periodicity, amplitude, and profile of the SdH oscillations, the density and quantum mobility (or lifetime) in different spin branches, together with the Rashba parameter, can be determined experimentally. These techniques are akin to those employed in the investigation of spin-degenerate 2DEGs in the presence of more than one occupied electronic subband[13,14]. It has been observed experimentally that in InAs- and InGaAs-based spintronic systems, although the electron densities can differ significantly in different spin branches[10～12], the quantum mobilities, determined from the amplitudes of the SdH oscillations at relatively low and intermediate magnetic fields, depend very weakly on the SOI strength[10]. This result is in sharp contrast to what has been seen in spin-degenerate (e.g., GaAs-based) 2DEGs with more than one occupied subband, where both quantum and transport mobilities differ significantly in different electronic subbands. In order to understand this important and interesting experimental finding and to achieve an in-depth understanding of how SOI affects the electronic and transport properties of a 2DEG, we develop a tractable theoretical approach to examine quantum and transport mobilities pertinent to a spin-split 2DEG in this paper.

2 One-particle aspects

For a typical 2DEG formed in the xy-plane (taken as the 2D-plane) in narrow-gap semiconductor nanostructures, such as InGaAs/InAlAs heterojunctions in which the growth-direction is taken along the z-axis, the effect of SOI can be obtained from a k · p band-structure calculation[1,5]. Including the lowest order of the SOI induced by the Rashba effect, the single-electron Hamiltonian is given, in the absence of electronic scattering centers, by

$$H_0 = \frac{p^2}{2m^*} + \frac{\alpha}{\hbar}(\sigma \times p)_z + U(z) \quad (1)$$

where $p = (p_x, p_y)$ is the momentum operator in which $p_x = -i\hbar\partial/\partial x$, m^* is the electron effective mass, $U(z)$ is the confining potential energy along the growth-direction, and α is the Rashba parameter which measures the strength of the spin-orbit coupling. Due to the Pauli spin matrices $\sigma = (\sigma_x, \sigma_y, \sigma_z)$, this Hamiltonian is a 2×2 matrix. Furthermore, this Hamiltonian suggests that the SOI induced by the Rashba effect does not affect the electronic states along the growth direction. The solutions of the corresponding Schrödinger equation are readily obtained[4] as

$$\Psi_{\sigma k n}(R) = |\sigma, k, n\rangle = \frac{1}{\sqrt{2}}\begin{pmatrix} 1 \\ i\sigma e^{i\phi} \end{pmatrix} e^{ik\cdot r}\psi_n(z) \quad (2)$$

where $k = (k_x, k_y)$ is the electron wavevector along the 2D plane, $R = (r, z) = (x, y, z)$, ϕ is the angle between k and the x-axis, and $\sigma = \pm 1$ refers to different spin branches in k-space. The corresponding energy spectrum is given by

$$E_{\sigma n}(k) = E_\sigma(k) + \varepsilon_n = \frac{\hbar^2 k^2}{2m^*} + \sigma\alpha k + \varepsilon_n \quad (3)$$

with $k = (k_y^2 + k_x^2)^{1/2}$. In Eqs. (2) and (3), the wavefunction $\psi_n(z)$ and energy ε_n for an electron in the nth electronic subband are determined by a spin-independent Schrödinger equation along the growth-direction, because SOI does not affect the electron states along the z-direction.

From the electron energy spectrum given by Eq. (3), one can immediately see that in the presence of the Rashba spin-splitting: (1) the electronic states are split into two spin branches in k-space and electrons are oriented perpendicular to the electronic momentum in the 2D-plane; (2) the energy dispersion of a 2DEG is not parabolic due to the inclusion of the SOI term; and (3) the energy levels for the ±spin branches depend strongly on electron wavevector (or momentum), where the energy separation between the two spin branches is a linear-in-k term. These features are in sharp contrast to those for a spin-degenerate 2DEG. Using Eq. (3), the Green's function for a spin-split 2DEG can be obtained, in the (E, k) or (spectrum, momentum) representation, as

$$G_{\sigma kn}(E) = [E - E_{\sigma n}(k) + i\delta]^{-1} \quad (4)$$

Thus, the density-of-states (DoS) for a spin-split 2DEG can be determined from the imaginary part of $G_{\sigma kn}(E)$. In this paper, we consider an InGaAs/InAlAs heterojunction in which only the lowest electronic subband is present (i.e., $n' = n = 0$), and we measure the energy from ε_0. In such a case, the electron DoS in different spin branches is obtained as

$$D_\sigma(E) = \sum_k \delta[E - E_\sigma(k)] \quad (5)$$

where for spin-up

$$D_+(E) = \frac{D_0}{2}\Theta(E)\left(1 - \sqrt{\frac{E_\alpha}{E + E_\alpha}}\right) \quad (6)$$

for spin-down

$$D_-(E) = \frac{D_0}{2}\left[\Theta(E)\left(1 + \sqrt{\frac{E_\alpha}{E + E_\alpha}}\right) + 2\Theta(-E)\Theta(E + E_\alpha)\sqrt{\frac{E_\alpha}{E + E_\alpha}}\right] \quad (7)$$

and the total DoS is

$$D(E) = D_+(E) + D_-(E) = D_0\left[\Theta(E) + \Theta(-E)\Theta(E + E_\alpha)\sqrt{\frac{E_\alpha}{E + E_\alpha}}\right] \quad (8)$$

Here, $\Theta(x)$ is the unit-step function, E is the electron energy, $D_0 = m^*/\pi\hbar^2$, and $E_\alpha = \alpha^2 m^*/2\hbar^2$. These theoretical results indicate that in contrast to a spin-degenerate 2DEG whose DoS is given simply by $D(E) = D_0\Theta(E)$, the DoS for a spin-split 2DEG depends strongly on SOI, which results in the following: (1) spin-up and spin-down electrons have different DoS; (2) the DoS depends not only on those step-functions but also on $E_\alpha = (E + E_\alpha)$, because of a nonparabolic energy spectrum given by Eq. (3); and (3) for the spin-down channel the DoS can exit even in the negative energy regime, whereas $D_+(E)$ only exits when $E > 0$. Furthermore, we note that $D_-(E)/D_0 = (\infty, 0.5]$ when $E = [E_\alpha, \infty)$, whereas $D_+(E)/D_0 = [0, 0.5]$ when $E = [0, \infty)$. This implies that $D_-(E)$ is always larger than $D_+(E)$ and a larger $D_+(E)$ can be observed at a larger E. These interesting features can be more clearly seen from Fig. 1 where the DoS in different spin-orbits is shown as a function of electron energy.

The theoretical results obtained and shown above indicate that in the low energy regime, which is most probably occupied by electrons, the DoS for the ‘ - ’ branch is always larger than that for the ‘ + ’ branch, and this is the main reason

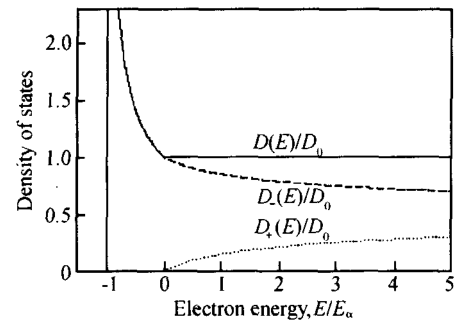

Fig. 1 Density-of-states in different spin branches ($D_\pm(E)$) as a function of electron energy E

why electron density in the spin-down channel is always larger than that in the spin-up channel. A direct and important application of the DoS for a spin-split 2DEG is to determine the Fermi energy of the system and the electron density in different spin branches. Applying the DoS for a 2DEG with SOI to the condition of total electron number conservation and the definition $n_\sigma = \sum_k f(E_\sigma(k))$ with $f(x)$ being the Fermi-Dirac function, the Fermi energy E_F and electron density n_σ in the σ spin branch are obtained, respectively, for low temperatures $T \to 0$, as

$$E_F = \frac{\hbar^2}{m^*}(\pi n_e - k_\alpha^2) \quad (9)$$

and

$$n_\sigma = \frac{n_e}{2} - \sigma\frac{k_\alpha}{2\pi}\sqrt{2\pi n_e - k_\alpha^2} \quad (10)$$

for $n_e \geq k_\alpha^2/\pi$ (or $\alpha \leq \hbar^2\sqrt{\pi n_e}/m^*$). Here, $n_e = n_- + n_+$ is the total electron density and $k_\alpha = m^*\alpha/\hbar^2$. For $= n_e \leq k_\alpha^2/\pi$ we have $E_F \leq 0$, and only the lower-energy ‘ - ’ spin branch is occupied by electrons (see Fig. 1), with $n_+ = 0$ and $n_- = n_e$ precisely at $n_e = k_\alpha^2/\pi$; in this case the electrons are entirely in the ‘ - ’ spin branch. However, it should be noted that the condition $n_e < k_\alpha^2/\pi$ can only be satisfied in a system with very low electron density and very large Rashba parameter, which has not yet been realized experimentally. Therefore, in this paper, we only consider the situation where both $\pm$ spin branches are occupied by electrons, namely the situation where $n_e > k_\alpha^2/\pi$. From Eq. (10), we obtain the relation

$$\sqrt{4\pi n_\sigma} + \sigma k_\alpha = \sqrt{2\pi n_e - k_\alpha^2} \quad (11)$$

which will be used later in the paper.

Another simple way to understand why the presence of SOI can lead to different electron densities in different spin branches is to look into

the dispersion relation $E_\sigma(k)$ versus k shown in Fig. 2. In Fig. 2, the solid parabolic curve corresponds to the absence of the SOI ($\alpha=0$), i.e., to $k_F^- = k_F^+ = k_F$. The intersections of the curves for $\alpha \neq 0$ ($E_+(k)$ and $E_-(k)$) with the Fermi level E_F, projected onto the k-axis, give the Fermi wavevectors k_F^- and k_F^+. The difference $k_F^- - k_F^+$ at $\alpha \neq 0$ leads to a difference in k-space area: $\pi(k_F^-)^2 \neq \pi(k_F^+)^2$. Accordingly, the densities n_- and n_+ are different when the SOI is present. Because k_F^- is always larger than k_F^+, n_- is always larger than n_+.

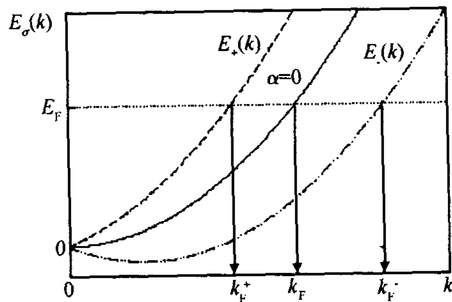

Fig. 2 Dispersion relation $E_\sigma(k)$ versus k for 2DEGs The solid parabolic curve, for $\alpha=0$, corresponds to the absence of SOI where $k_F^+ = k_F^- = k_F$. The intersections of the dashed curves ($E_\pm(k)$) for $\alpha \neq 0$ with the Fermi level E_F (dotted line), projected onto the k-axis, give the Fermi wavevectors k_F^- and k_F^+ for different spin branches.

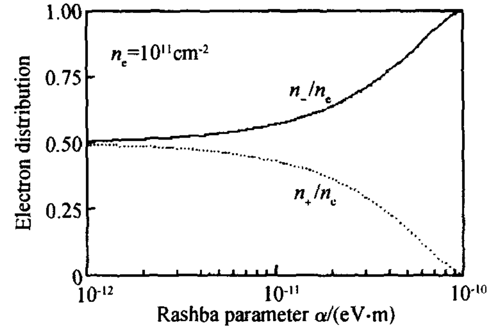

Fig. 3 Electron density n_σ in different spin channels as a function of the Rashba parameter α at a fixed total electron density $n_e = n_+ + n_-$

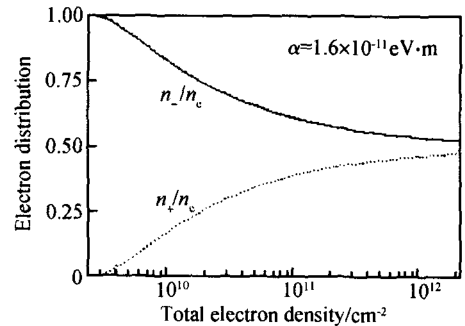

Fig. 4 Dependence of electron distribution in the ±spin branches on total electron density at a fixed Rashba parameter

The dependence of electron distribution in different spin branches on the Rashba parameter α and total electron density n_e is shown respectively in Figs. 3 and 4. These results are obtained for an InGaAs-based 2DEG structure. It should be noted that with increasing α in Fig. 3 and/or decreasing n_e in Fig. 4, Fermi energy decreases (see Eq. (9)) and, consequently, more electrons are in the spin-down orbit because it has a lower energy and higher DoS. This is in line with experimental findings[8,10~12]. The results shown in Figs. 3 and 4, together with those given by Eqs. (6) and (7), suggest that in a 2DEG, spin polarization increases with increasing Rashba parameter and/or with decreasing total electron density.

3 Electron-impurity scattering

At low temperatures, electron-impurity scattering is the principal channel for the relaxation of electrons in semiconductor-based 2DEG systems. For a modulation-doped InGaAs/InAlAs heterojunction, the main sources of electron-impurity scattering come from the ionized remote-impurities in the InAlAs layer and from the charged background impurities in the InGaAs layer. The Coulomb potential induced by electron interaction with charged impurities takes the form

$$V(R - R_a) = \frac{Ze^2}{\kappa} \times \frac{1}{|R - R_a|} \tag{12}$$

where the impurity is located at $R_a = (r_a, z_a) = (x_a, y_a, z_a)$, Z is its charge number, and κ is the static dielectric constant of the material. In the absence of electron-electron (e-e) screening, this potential results in an electron-impurity interaction Hamiltonian in momentum representation after the Fourier transformation

$$H_{e\text{-}i} = \frac{2\pi Ze^2}{\kappa q} e^{-q|z-z_a|} e^{iq\cdot(r-r_a)} \tag{13}$$

where $q = (q_x, q_y)$ is the factor of the Fourier transform, which corresponds to the change of electron wavevector (or momentum) during an

electron-impurity scattering event. For electron interactions with charged impurities in an electronic system, we may assume that the system under study can be separated into the electron of interest and the impurities, i.e., $|\sigma, k, n; c\rangle = |\sigma, k, n\rangle |c\rangle$ where $|c\rangle$ represents the state of the impurity system. Thus, the matrix element for electron-impurity interaction is obtained as

$$U^0_{n n',\sigma\sigma'}(q, R_a) = \frac{2\pi Ze^2}{\kappa q}\sqrt{n_i(z_a)} \times F_{n n'}(q, z_a)\, h_{\sigma\sigma'}(\theta)\, e^{-iq\cdot r_a}\delta_{k',k+q} \quad (14)$$

Here, $n_i(z_a) = |\langle c|c\rangle|^2$ is the impurity distribution along the growth-direction under the assumption that the impurities are uniformly distributed along the xy-plane, $F_{nn'}(q, z_a) = \int dz \psi^*_{n'}(z) \times \psi_n(z) e^{-q|z-z_a|}$ is the form factor for electron-impurity scattering in a 2D system, and $h_{\sigma\sigma'}(\theta) = [1 + \sigma\sigma' \times (\cos\theta - i\sin\theta)]/2$ is a spin-dependent matrix element with θ being the angle between k' and k. For the case where only the lowest electronic subband is present, we have

$$U^0_{\sigma\sigma'}(q, R_a) = \frac{2\pi Ze^2}{\kappa q}\sqrt{n_i(z_a)} \times F_0(q, z_a)\, h_{\sigma\sigma'}(\theta)\, e^{-iq\cdot r_a}\delta_{k',k+q} \quad (15)$$

with $F_0(q, z_a) = \int dz |\psi_0(z)|^2 e^{-q|z-z_a|}$. From Eqs. (14) and (15), we see that similar to a spin-degenerate 2DEG, the element of the electron-impurity interaction matrix diverges in a spin-split 2DEG when $q \to 0$. Hence, it is necessary to include the effect of e-e screening on electron-impurity scattering.

4 Dielectric function matrix and screening length

We now study the many-body effects of a 2DEG in the presence of SOI. Applying the electron wavefunction given by Eq. (2) to the e-e interaction Hamiltonian induced by the Coulomb potential, the space Fourier transform of the matrix element for bare e-e interaction can be written as

$$V_{\sigma_1\sigma_2\sigma_3\sigma_4, n_1 n_2 n_3 n_4}(k, q) = \delta_{k'+k, k_1'+k_1} V_q \int d^3R_1 \int d^3R_2\, \Psi^*_{\sigma_1 k n_1'}(R_1)\Psi^*_{\sigma_2 k n_2}(R_1) \times e^{iq(r_1-r_2)} e^{-q|z_1-z_2|}\Psi_{\sigma_3 k_1 n_3}(R_2)\Psi_{\sigma_4 k_1 n_4}(R_2) \quad (16)$$

where $V_q = 2\pi e^2/\kappa q$. From now on, we consider an InGaAs/InAlAs heterojunction in which only the lowest electronic subband is present. After defining $\beta = (\sigma\sigma')$ for electronic transition from the σ' branch to the σ branch, the bare e-e interaction in the presence of SOI becomes

$$V_{\beta\gamma}(k, q) = V_q G_0(q) \times \left[\frac{1+\beta A_{kq}}{2}\delta_{\beta\gamma} + \frac{i\beta B_{kq}}{2}(1-\delta_{\beta\gamma})\right] \quad (17)$$

where $G_0(q) = \int dz_1 \int dz_2 |\psi_0(z_1)|^2 |\psi_0(z_2)|^2 e^{-q|z_1-z_2|}$ with $\psi_0(z)$ being the ground-state electron wavefunction along the growth-direction, $A_{kq} = (k + q\cos\psi)/|k+q|$, $B_{kq} = q\sin\psi/|k+q|$, and ψ is the angle between k and q. It should be noted that in contrast to a spin-degenerate 2DEG for which the bare e-e interaction does not depend on k[15], $V_{\beta\gamma}(k, q)$ for a spin-split 2DEG depends not only on q but also on k, because the spin splitting depends explicitly on k.

From the electron energy spectrum given by Eq. (3), we can derive the retarded and advanced Green functions for electrons when the effect of SOI is taken into consideration. Applying these Green functions along with the bare e-e interaction to the diagrammatic techniques to derive effective e-e interaction under the random-phase approximation (RPA), we obtain the effective e-e interaction as[16]

$$V^{eff}_{\beta\gamma}(\Omega; k, q) = \epsilon^{-1}_{\beta\gamma}(\Omega; k, q)\, V_{\beta\gamma}(k, q) \quad (18)$$

Here,

$$\epsilon_{\beta\gamma}(\Omega; k, q) = \delta_{\beta\gamma}\delta(k) - V_{\beta\gamma}(k, q)\Pi_\gamma(\Omega; k, q) \quad (19)$$

is the dynamical dielectric function matrix element and

$$\Pi_{\sigma\sigma'}(\Omega; k, q) = \frac{f[E_{\sigma'}(k+q)] - f[E_\sigma(k)]}{\hbar\Omega + E_{\sigma'}(k+q) - E_\sigma(k) + i\delta}$$

is the pair bubble or density-density correlation function in the absence of e-e interaction, with $f(x)$ being the Fermi-Dirac function. For a spin-split 2DEG, the effective e-e interaction and the dielectric function matrix depend not only on q but also on k, in contrast to a spin-degenerate 2DEG. After summing the dielectric function matrix over k and noting $\sum_k B_{kq}\Pi_{\sigma\sigma'}(\Omega; k, q) = 0$, the dielectric function matrix for a 2DEG with Rashba spin splitting is obtained as

$$\epsilon(\Omega, q) = \begin{bmatrix} 1+a_1 & 0 & 0 & a_4 \\ 0 & 1+a_2 & a_3 & 0 \\ 0 & a_2 & 1+a_3 & 0 \\ a_1 & 0 & 0 & 1+a_4 \end{bmatrix} \quad (20)$$

Here, the indexes $1 = (++)$, $2 = (+-)$, $3 =$

(- +) and 4 = (- -) are defined in regard to different transition channels and $a_j = a_j(\Omega, q) = -(V_q F_0(q)/2)\sum_k (1 \pm A_{kq})\Pi_j(\Omega; k, q)$ where the upper (lower) case refers to j = 1 or 4 for intra-SO transition (j = 2 or 3 for inter-SO transition). Moreover, the inverse dielectric function matrix for a spin-split 2DEG is

$$\epsilon^{-1}(\Omega, q) = \begin{bmatrix} 1 - a_1^* & 0 & 0 & -a_4^* \\ 0 & 1 - a_2^* & -a_3^* & 0 \\ 0 & -a_2^* & 1 - a_3^* & 0 \\ -a_1^* & 0 & 0 & 1 - a_4^* \end{bmatrix} \tag{21}$$

where $a_1^* = a_1/(1 + a_1 + a_4)$, $a_2^* = a_2/(1 + a_2 + a_3)$, $a_3^* = a_3/(1 + a_2 + a_3)$, and $a_4^* = a_4/(1 + a_1 + a_4)$.

With the inverse dielectric function matrix, we can calculate the matrix element for the electron-impurity interaction in the presence of e-e screening, through the definition $U_i(q, R_a) = \sum_j \epsilon_{ij}^{-1}(q) U_j^0(q, R_a)$. Here $\epsilon_{ij}(q) = \epsilon_{ij}(\Omega \to 0, q)$ is the element of the static dielectric function matrix. Using Eq. (15), the square of the matrix element for the electron-impurity interaction in the presence of e-e screening becomes

$$|U_1(q,\theta)|^2 = |U_4(q,\theta)|^2 = |U_+(q,\theta)|^2 \delta_{k',k+q} \tag{22}$$

for intra-SO scattering, and

$$|U_2(q,\theta)|^2 = |U_3(q,\theta)|^2 = |U_-(q,\theta)|^2 \delta_{k',k+q} \tag{23}$$

for inter-SO scattering. Here,

$$|U_\pm(q,\theta)|^2 = \left(\frac{2\pi Ze^2}{k}\right)^2 \frac{h_\pm(\theta)}{[q + K_\pm(q)]^2} \times \int z_a n_i(z_a) F_0^2(q, z_a) \tag{24}$$

in which the contribution from the impurity distribution along the growth direction has been summed over, $h_\pm(\theta) = (1 \pm \cos\theta)/2$, and the inverse screening lengths for intra- and inter-SO electronic transitions are, respectively,

$$K_+(q) = q[a_1(q) + a_4(q)] = -\frac{q}{2} V_q G_0(q) \sum_{\sigma, k}(1 + A_{kq}) \times \frac{f[E_\sigma(k+q)] - f[E_\sigma(k)]}{E_\sigma(k+q) - E_\sigma(k)} \tag{25}$$

and

$$K_-(q) = q[a_2(q) + a_3(q)] = -\frac{q}{2} V_q G_0(q) \sum_{\sigma, k}(1 + A_{kq}) \times \frac{f[E_\sigma(k+q)] - f[E_{-\sigma}(k)]}{E_\sigma(k+q) - E_{-\sigma}(k)} \tag{26}$$

After carrying out the angle integration, we have

$$K_\pm(q) = \frac{16 e^2 m^*}{\pi \hbar^2 \kappa q} G_0(q) \sum_\sigma \int_0^\infty dk \times \frac{f[E_\sigma(k)]k(k+q)}{(2k + q + 2\sigma k_\alpha)(k + q + |k - q|)} H_\sigma^\pm(k, q) \tag{27}$$

where

$$H_\sigma^\pm(k, q) = \frac{-1 \pm 1}{2} K(A) + \Pi(AB_\pm, A) + \frac{q(q + 2\sigma k_\alpha)}{4k(k + \sigma k_\alpha)}[\Pi(AC_\pm, A) - \Pi(AB_\pm, A)] \tag{28}$$

$K(x)$ is a complete elliptic integral of the first kind, $\Pi(n, x) = \Pi(\pi/2, n, x)$ is a complete elliptic integral of the third kind, $A = (k + q - |k - q|)/(k + q + |k - q|)$, $B_\pm = [(2k + q)/q]^{\pm 1}$, and $C_\pm = [(q - 2\sigma k_\alpha) = (2k + q + 2\sigma k_\alpha)]^{\pm 1}$. For the case of a low-temperature limit (i.e., $T \to 0$), we obtain

$$K_\pm(q) = \frac{16 e^2 m^*}{\pi \hbar^2 \kappa q} G_0(q) \sum_\sigma \int_0^{\sqrt{4\pi n_\sigma}} dk \times \frac{k(k+q)}{(2k + q + 2\sigma k_\alpha)(k + q + |k - q|)} H_\sigma^\pm(k, q) \tag{29}$$

These results imply that in the presence of SOI, the intra- and inter-SO transitions have different screening lengths under the RPA approach. In particular, we note that in a long wavelength limit (i.e., $q \to 0$ which means that the e-e interaction does not change the electron wavevector or momentum), $K_+(q) \to \infty$ whereas $K_-(q) \to 0$.

5 Spin-dependent quantum and transport mobilities

From the above presented results, we obtain for the electronic transition rate given by Fermi's golden rule

$$W_{\sigma'\sigma}(k', k) = \frac{2\pi}{\hbar} |U_{\sigma'\sigma}(q,\theta)|^2 \delta_{k',k+q} \delta[E_{\sigma'}(k') - E_\sigma(k)] \tag{30}$$

which is the probability for an electron to be scattered from a state $|\sigma, k\rangle$ to a state $|\sigma', k'\rangle$ due to screened electron-impurity scattering. We now consider a weak DC electric field F_x applied along the 2D-plane (taken along the x direction) of a 2DEG. In the steady state the corresponding semi-classical Boltzmann equation, for nondegenerate statistics, reads

$$-\frac{eF_x}{\hbar}\times\frac{\partial f_\sigma(k)}{\partial k_x} = \sum_{k',\sigma'}[f_{\sigma'}(k')W_{\sigma\sigma'}(k,k') - f_\sigma(k)W_{\sigma'\sigma}(k',k)] \tag{31}$$

where $f_\sigma(k)$ is the momentum-distribution function for an electron at a state $|\sigma,k>$. We assume that $f_\sigma(k)$ can be described by the drifted energy distribution function $f_\sigma(k) = f(E_\sigma(k_x - m^* v_\sigma/\hbar, k_y))$, where v_σ is the average drift-velocity of an electron in the σ spin branch along the x direction due to the presence of F_x. Then the momentum-balance equation[17,18] can be derived by multiplying k_x with both sides of the Boltzmann equation and by summing over k. In doing so, we have

$$\frac{eF_x}{\hbar}n_\sigma = \sum_{\sigma'}\sum_{k,k'}[k_x f_{\sigma'}(k')W_{\sigma\sigma'}(k',k) - k_x f_\sigma(k)W_{\sigma'\sigma}(k',k)] \tag{32}$$

For weak driving fields F_x we assume $v_\sigma \ll \hbar k_x/m^*$ and obtain

$$f_\sigma(k) \simeq f(E_\sigma(k)) - \hbar k_x v_\sigma(1+\sigma k_\alpha/k)f'(E)|_{E=E_\sigma(k)} \tag{33}$$

where $f'(E) = \partial f(E)/\partial E$. Thus the momentum-balance equation gives

$$n_\sigma = \sum_{\sigma'}[\mu_t^\sigma B_{\sigma\sigma'} - \mu_t^{\sigma'}C_{\sigma\sigma'}] \tag{34}$$

Here $\mu_t^\sigma = v_\sigma/F_x$ is the transport mobility for an electron in spin branch σ and

$$\begin{pmatrix}B_{\sigma\sigma'}\\C_{\sigma\sigma'}\end{pmatrix} = -\frac{\hbar^2}{e}\sum_{k,k'}\begin{pmatrix}k_x\\k'_x\end{pmatrix}\times k_x(1+\sigma k_\alpha/k)W_{\sigma'\sigma}(k',k)f'(E)|_{E=E_\sigma(k)} \tag{35}$$

It can be seen that the term $B_{\sigma\sigma'}$ is induced by small-angle scattering between k' and k. Hence, by definition, the quantum mobility of electrons in spin branch σ, μ_q^σ, is given by

$$\frac{1}{\mu_q^\sigma} = \frac{1}{n_\sigma}\sum_{\sigma'}B_{\sigma\sigma'} \tag{36}$$

The transport mobility, μ_t^σ, in different spin branches can be determined by solving Eq. (34), which reads

$$\mu_t^+ = \frac{(B_4 - C_4 + B_2)n_+ + C_2 n_-}{(B_1 - C_1 + B_3)(B_4 - C_4 + B_2) - C_2C_3} \tag{37}$$

and

$$\mu_t^- = \frac{C_3 n_+ + (B_1 - C_1 + B_3)n_-}{(B_1 - C_1 + B_3)(B_4 - C_4 + B_2) - C_2C_3} \tag{38}$$

Here, again, 1 = (+ +), 2 = (+ -), 3 = (- +) and 4 = (- -) correspond to different channels for electronic transition. From the quantum and transport mobilities, the quantum and transport lifetimes for an electron in different spin branches are given respectively by $\tau_q^\sigma = m^*\mu_q^\sigma/e$ and $\tau_t^\sigma = m^*\mu_t^\sigma/e$. Furthermore, the average transport mobility, measured in a conventional transport experiment, is given as

$$\mu_t = \frac{n_+\mu_t^+ + n_-\mu_t^-}{n_e} \tag{39}$$

Using Eq. (30) we obtain, for electron-impurity scattering,

$$\begin{pmatrix}B_{\sigma\sigma'}\\C_{\sigma\sigma'}\end{pmatrix} = \frac{-m^*}{4\pi^2\hbar e}\int_0^\pi d\theta\int_0^\infty dk\, k_{\sigma\sigma'}k\begin{pmatrix}k\\k_{\sigma\sigma'}\cos\theta\end{pmatrix}\times |U_{\sigma\sigma'}(q,\theta)|^2 f'(E)|_{E=E_\sigma(k)} \tag{40}$$

Here, $q = \sqrt{k_{\sigma\sigma'}^2 + k^2 - 2kk_{\sigma\sigma'}\cos\theta}$ and $k_{\sigma\sigma'} = k - (\sigma' - \sigma)k_\alpha$. For low temperatures, i.e., for $T\to 0$, we have $f'(E) = \partial f(E)/\partial E \approx -\delta(E_F - E)$ with E_F being the Fermi energy. Then we obtain

$$\begin{pmatrix}B_{\sigma\sigma'}\\C_{\sigma\sigma'}\end{pmatrix} = \frac{m^{*2}}{4\pi^2\hbar^3 e}\times\frac{kk_{\sigma\sigma'}}{k+\sigma k_\alpha}\int_0^\pi d\theta\begin{pmatrix}k\\k_{\sigma\sigma'}\cos\theta\end{pmatrix}\times |U_{\sigma\sigma'}(q,\theta)|^2|_{k=\sqrt{4\pi n_\sigma}} \tag{41}$$

After using Eq. (11), for different transition channels we have

$$\begin{pmatrix}B_1\\C_1\end{pmatrix} = 2c_0(n_+/n_-)^{1/2}(n_+/n_e)\times\int_0^\pi d\theta\begin{pmatrix}1\\\cos\theta\end{pmatrix}|U_+(q_1,\theta)|^2 \tag{42}$$

with $c_0 = m^{*2}n_e\sqrt{4\pi n_-}/(2\pi\hbar^3 e\sqrt{2\pi n_e - k_\alpha^2})$ and $q_1 = 4\sqrt{\pi n_+}\sin(\theta/2)$,

$$\begin{pmatrix}B_2\\C_2\end{pmatrix} = c_0\int_0^\pi d\theta\begin{pmatrix}1\\\sqrt{n_+/n_-}\cos\theta\end{pmatrix}|U_-(q_-,\theta)|^2 \tag{43}$$

with $q_- = 2\sqrt{\pi n_e - (\pi n_e - k_\alpha^2)\cos\theta}$,

$$\begin{pmatrix}B_3\\C_3\end{pmatrix} = c_0\int_0^\pi d\theta\begin{pmatrix}\sqrt{n_+/n_-}\\\cos\theta\end{pmatrix}|U_-(q_-,\theta)|^2 \tag{44}$$

and

$$\begin{pmatrix}B_4\\C_4\end{pmatrix} = 2c_0(n_-/n_e)\int_0^\pi d\theta\begin{pmatrix}1\\\cos\theta\end{pmatrix}|U_+(q_4,\theta)|^2 \tag{45}$$

with $q_4 = 4\sqrt{\pi n_-}\sin(\theta/2)$. These results indicate that corresponding to different electronic transition channels due to electron-impurity scattering, the change of the electron wavevector or momentum q is different. For intra-SO scattering, $k_1 = \sqrt{4\pi n_+}$ and $q = q_1 = [0, 4\sqrt{\pi n_+}]$ for a transition within the '+' spin branch, and $k_4 = \sqrt{4\pi n_-}$ and

$q = q_4 = [0, 4\sqrt{\pi n_-}]$ for a transition within the '−' branch. Whereas for inter-SO scattering, $q = q_- = [2k_\alpha, 2\sqrt{2\pi n_e - k_\alpha^2}]$ is the same for both a transition from the '+' spin branch to the '−' branch and a transition from the '−' branch to the '+' branch. Furthermore, $q \to 0$ can only be a case for intra-SO scattering. For inter-SO scattering, $q \neq 0$, which implies that an inter-SO transition can only be achieved via varying the wavevector (or momentum) of an electron, because the spin-splitting depends explicitly on electron wavevector.

6 InGaAs/InAlAs heterojunction

In an InGaAs/InAlAs heterojunction, the impurity scattering comes mainly from: (1) ionized remote impurities within a narrow space charge layer in the InAlAs region with a concentration N_r at a spacer distance s from the interface, due to modulation-doping; and (2) charged background impurities with a depletion charge density N_{depl} and a depletion length d in the InGaAs layer, due to the effect of depletion. In general, these impurity concentrations and their distributions along the growth-direction are not well known, because the ionization of modulation-doped impurities (including deep-centers) and the depletion length and charge density of the background impurities are not easily determined experimentally. In conjunction with a typical spintronic device realized from an InGaAs/InAlAs heterojunction[7], in this paper we model the remote and background impurity distributions respectively as

$$n_r(z_a) = N_r \delta(z_a + s) \tag{46}$$

and

$$n_b(z_a) = (N_{depl}/d)\Theta(z_a) \tag{47}$$

These assumptions are mainly based on the fact that the width of the charge layer for modulation-doping is relatively narrow and the depletion length in the InGaAs layer is much longer than the effective thickness of the confining potential for electrons.

In the present work, we apply the usual triangular well approximation to model the confining potential normal to the interface of the heterojunction and use the corresponding variational wave function for the ground subband[15]. Thus, the square of the electron-impurity interaction matrix element induced by scattering with remote and background impurities is given respectively by

$$|U_\pm^r(q,\theta)|^2 = N_r\left(\frac{2\pi Ze^2}{k}\right)^2 \times \frac{h_\pm(\theta)}{[q + K_\pm(q)]^2} \times \frac{e^{-2qs}}{(x+1)^6} \tag{48}$$

and

$$|U_\pm^b(q,\theta)|^2 = N_b\left(\frac{2\pi Ze^2}{k}\right)^2 \frac{h_\pm(\theta)}{[q + K_\pm(q)]^2} \times \frac{3x^5 + 18x^4 + 43x^3 + 48x^2 + 24x + 2}{4x(x+1)^6} \tag{49}$$

where $x = q = b$, $N_b = N_{depl}/db$ and $b = [(48\pi m^* \times e^2/k\hbar^2](N_{depl} + 11n_e/32)]^{1/3}$ defines the thickness ($\simeq 3/b$) of the triangular well. These results indicate that similar to a spin-degenerate 2DEG, electrons in a heterojunction interact more strongly with background impurities than with remote impurities, especially when $q \to 0$. This is mainly due to the fact that background impurities are located in the layer where the majority of conducting electrons are. The form factor for the e-e interaction is

$$G_0(q) = \frac{3x^2 + 9x + 8}{8(x+1)^3} \tag{50}$$

7 Numerical results and discussion

The results of this section pertain to InGaAs/InAlAs heterojunctions at low temperatures. The material parameters corresponding to InGaAs are taken as follows: (1) electron effective mass $m^* = 0.042\, m_e$ with m_e being the rest-mass of an electron; (2) static dielectric constant $k = 12.9$; and (3) the typical depletion charge density $N_{depl} = 2 \times 10^{10}\ \mathrm{cm}^{-2}$. Furthermore, the electron distribution $n_\pm$ in different spin branches is determined using Eq. (10) (also see Figs. 3 and 4). In the calculations, the charge number of an impurity is taken to be $Z = 1$.

7.1 Screening length

From the results presented in Section 5, we know that for electron-impurity scattering at low-temperatures, the change of electron wavevector or momentum (i.e., q depends on electron density n_σ and angle θ) differs for different transition channels. Thus, in order to study the effect of e-e interaction on transport coefficients induced by electron-impurity scattering, it is convenient and useful to look into the angular dependence of the

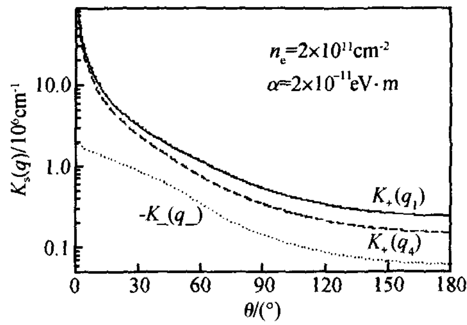

Fig.5 Inverse screening length $K_s(q)$, $s = \pm$, for transition within the '±' spin branch as a function of angle θ at a fixed total electron density n_e and a fixed Rashba parameter α Here, θ is the angle between the initial electronic wavevector (or momentum) k and the final wavevector k′, $q_1 = 4\sqrt{\pi n_+}\sin(\theta/2)$ for a transition within the '+' branch, $q_4 = 4\sqrt{\pi n_-}\sin(\theta/2)$ for a transition within the '-' branch, $q_- = 2\sqrt{\pi n_e - (\pi n_e - k_\alpha^2)\cos\theta}$ for inter-SO transition, and $n_\pm$ is the electron density in the '±' spin branch. Note that $K_-(q_-)$ is negative.

screen length for different transition channels. In Fig. 5, the inverse screening length $K_\pm(q)$ is shown as a function of θ (the angle between the initial wavevector k and the final wavevector k′ during a scattering event) at a fixed total electron density n_e and a fixed Rashba parameter α. From these results, we note that: (1) $|K_\pm(q)|$ decreases with increasing θ, which implies that a strong effect of e-e screening can be achieved at small scattering angles; (2) for intra-SO transition within the '+' or '-' spin branch, $K_+(q) \to +\infty$ when $\theta \to 0$ (i.e., $q \to 0$); (3) $K_-(q)$ for inter-SO transition is negative and finite when $\theta = [0, \pi]$; (4) at a fixed θ, $K_+(q_1)$ for a transition within the '+' branch is always larger than $K_+(q_4)$ for a transition with in the '-' branch; and (5) at a fixed θ, the inverse screening lengths induced by intra-SO transitions, $K_+(q_1)$ and $K_+(q_4)$, are much larger than $|K_-(q_-)|$ induced by inter-SO transition. Moreover, it should be noted that at a fixed θ, because the transition from the '-' spin branch to the '+' spin branch corresponds to the same q as for the transition from the '+' branch to the '-' branch, the screening length is the same for inter-SO transition channels.

The influence of the strength of SOI and total electron density on angular dependence of the inverse screening length is shown in Figs. 6 and 7, respectively, for transitions within the '+' and '-' spin channels. These results indicate that for intra-SO transitions, $K_+(q)$ increases with increasing α or with decreasing n_e. Together with those obtained for electron distribution (or spin polarization) shown in Figs. 3 and 4, an important conclusion we can draw is that the inclusion of

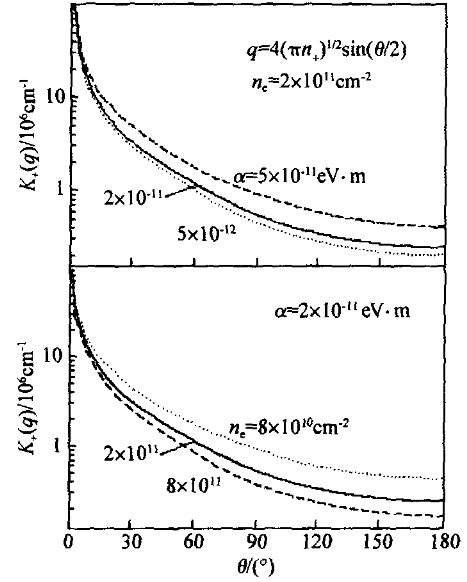

Fig. 6 Angular dependence of inverse screening length $K_+(q)$ for transition within the '+' spin branch The results are shown at a fixed total electron density n_e for different Rashba parameters α (upper panel) and at a fixed α for different n_e (lower panel).

SOI can enhance the effect of e-e screening in a 2DEG for intra-SO transitions. From Figs. 6 and 7, we note that $K_+(q_1)$ (induced by a transition within the '+' branch) depends more strongly on α and n_e than $K_+(q_4)$ (by a transition within the '-' branch) does. The dependence of the inverse screening length induced by an inter-SO transition on the Rashba parameter and total electron density is shown in Fig. 8. We see that in the small θ regime $-K_-(q)$ increases with decreasing α or increasing n_e, whereas at large θ, $-K_-(q)$ increases with increasing α or decreasing n_e. Thus, for inter-SO transitions, the SOI can reduce the effect of e-e screening in the small angle regime and enhance the screening effect at large θ.

The results shown in Figs. 5～8 indicate that in the presence of SOI, the screening length of a 2DEG differs significantly for different electronic transition channels. In particular, the e-e screen-

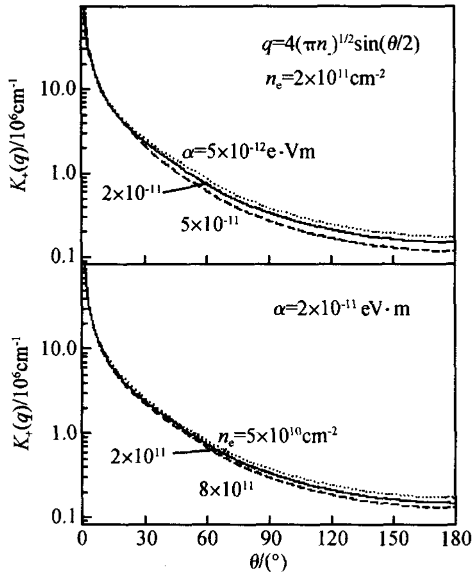

Fig. 7　Inverse screening length $K_+(q)$ for a transition within the ‘ - ’ spin branch as a function of θ In upper (lower) panel, the results are shown at a fixed total electron density n_e for different Rashba parameters α (at a fixed α for different n_e).

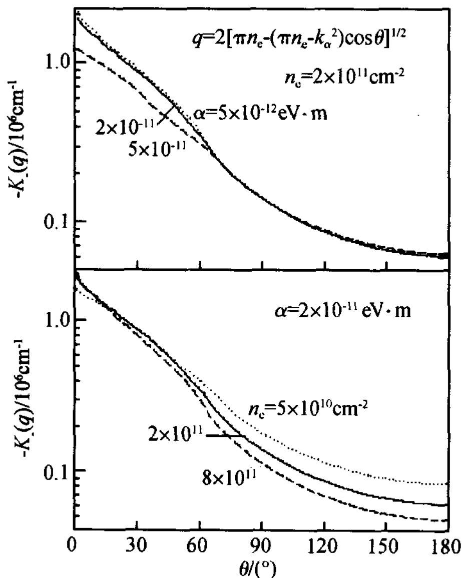

Fig. 8　Angular dependence of the inverse screening length for an inter-SO transition　Note that $K_-(q) < 0$ and $K_-(q)$ is the same for transitions from the ‘ - ’ branch to the ‘ + ’ branch and from the ‘ + ’ branch to the ‘ - ’ branch. The upper (lower) panel shows the results at a fixed total electron density (Rashba parameter) for different Rashba parameters (total electron densities).

ing affects more strongly the intra-SO transitions. The main physical reason behind this important effect is that the inter-SO transition due to e-e interaction requires the change of electron wavevector or momentum, because, again, the spin-splitting depends explicitly on electron wavevector. Furthermore, over a wide regime of θ or q, $|K_\pm(q)| \approx 10^5 \sim 10^6\ \mathrm{cm}^{-1}$, similar to the inverse screening length for a spin-degenerate 2DEG.

7.2　Quantum and transport mobilities

Here we study the quantum and transport mobilities in different spin branches due to electron interactions with remote and background impurities in an InGaAs/InAlAs heterojunction. Although the concentrations N_r and N_b for remote and background impurities are normally not known, one may assume that $N_r \propto n_e$ and $N_r \gg N_b$. The former assumption is based on the fact that the conducting electrons in the InGaAs layer come mainly from ionized donors modulation-doped in the InAlAs layer. The later assumption is made for the case of a high quality sample in which the background impurity concentration in the InGaAs layer is low. As has been shown in Section 6, electrons in a heterojunction interact more strongly with background impurities than with remote impurities. Hence, although the concentration N_b is relatively low, background impurities can significantly affect the transport properties of a sample.

From the results presented in Sections 5 and 6, we know that the square of the matrix element for electron-impurity scattering via inter-SO transition is not divergent over the whole defined regime of q or θ. Together with the fact that the e-e screening relatively weakly affects the inter-SO transition (see Figs. 5～8), in the present study we only include the effect of e-e screening for an intra-SO transition induced by electron-impurity scattering. Substituting n_σ in Eqs. (42)～(45) the factors $B_{\sigma\sigma}$ and $C_{\sigma\sigma'}$ induced by scattering with remote and background impurities can be calculated. Then the quantum and transport mobilities in different spin branches can be obtained, respectively, by using Eqs. (36)～(38). Moreover, the average transport mobility is given by Eq. (39).

The dependence of the quantum and transport mobilities in different spin channels, μ_q^σ and μ_t^σ, on the Rashba parameter α is presented in

Fig. 9 for the fixed n_e (total electron density), N_r and N_b (remote and background impurity concentration), and s (spacer thickness). We see that over a wide range of α, the differences between the quantum mobilities μ_q^+ and μ_q^- and between the transport mobilities μ^+ and μ^- are relatively small, in contrast to the electron distribution shown in Fig. 3. A pronounced difference between μ_q^+ and μ_q^- and between μ^+ and μ^- can only be observed at relatively large values of α. It can be seen that the difference between μ^+ and μ^- depends more strongly on α than that between μ_q^+ and μ_q^- does, especially at large values of α. At a large value of α, most of electrons are in the '-' spin branch (see Fig. 3) and, consequently, the average transport mobility μ is determined mainly by n_- and μ^-. It is interesting to note that similar to a spin-degenerate 2DEG[19], the transport mobility μ is much larger (about 5 times) than the quantum mobility $\mu^{\pm}$ in a spin-split 2DEG. Again, similar to a spin-degenerate 2DEG with more than one occupied electronic subband, where larger transport mobilities have been found in lower electronic subbands[20], a larger transport mobility can be observed at a lower energy-level, here the '-' spin branch in a 2DEG with SOI.

The physical reason behind the rather small difference of the electronic quantum mobilities in different spin branches is that, in contrast to a spin-degenerate 2DEG with more than one and fully quantized occupied subbands, the strength of the SOI and the separation of the $\pm$ branches in a 2DEG with SOI depend heavily on the electron wavevector k. Because the quantum mobility measures the strength of small-angle scattering, assessed experimentally from the SdH oscillations via the Dingle plot[19], elastic and small-angle scattering implies a small momentum exchange between the two spin branches during a scattering event. As a result, the difference in the quantum mobilities between the two spin branches is relatively small in comparison to that in the transport mobilities. Roughly the same quantum mobility in different spin branches have been observed experimentally in InGaAs-based 2DEG systems[10]. The results shown in Fig. 9 suggest that a much larger α is required in order to see a significant difference between μ_q^+ and μ_q^-.

The dependence of μ_q^{σ} and μ^{σ} on α is shown in

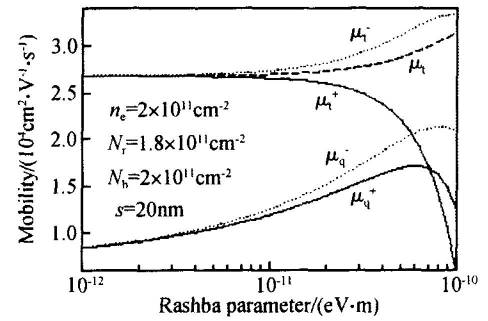

Fig. 9 Quantum and transport mobilities in the $\pm$ spin branches, $\mu_q^{\pm}$ and $\mu^{\pm}$, as a function of the Rashba parameter (α) for the fixed total electron density (n_e), remote and background impurity concentration (N_r and N_b) and spacer distance (s) Here μ is the average transport mobility (see Eq. (39)).

Fig. 10 at a fixed remote impurity concentration N_r for different background impurity concentrations N_b. We see that although N_b here is much smaller than N_r, the background impurity density strongly affects the value of the quantum and transport mobilities. This feature is in line with that observed in a spin-degenerate 2DEG. It can be found from Fig. 10 that with increasing the strength of the background impurity scattering (i.e., increasing N_b), the difference between μ_q^+ and μ_q^- and even between μ^+ and μ^- can become smal-

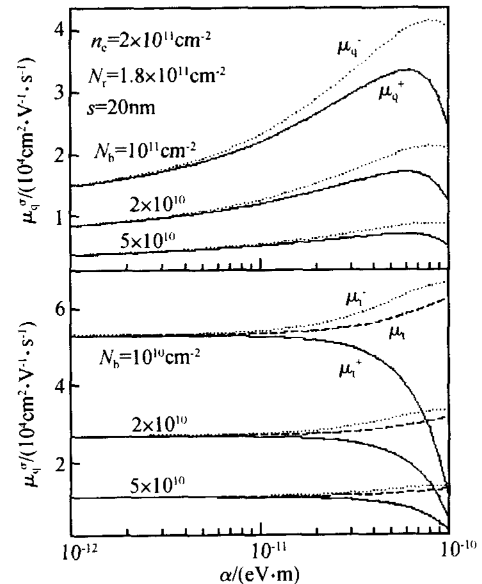

Fig. 10 Quantum and transport mobilities ($\mu_q^{\pm}$ and $\mu^{\pm}$ in the upper and lower panel) in different spin branches as a function of the Rashba parameter α at a fixed remote impurity concentration N_r for different background impurity concentrations N_b Here, n_e is the total electron density and s is the spacer distance.

ler. This is mainly due to the fact that electrons in a heterojunction interact more strongly with background impurities, especially for small-angle (or small q) scattering, as has been shown in Section 6. These results confirm further that small-angle scattering in a spin split 2DEG can reduce the difference between μ_q^+ and μ_q^-.

The dependence of $\mu_q^{\pm}$ and $\mu^{\pm}$ on total electron density n_e is shown in Fig. 11 at a fixed remote impurity density N_r for different background impurity concentrations N_b. At high electron densities the difference between μ_q^+ and μ_q^- and between μ_t^+ and μ_t^- is suppressed because of a small difference in the electron distribution in different spin branches (see Fig. 4). A significant difference between μ_q^+ and μ_q^- and between μ^+ and μ^- can be seen at low electron densities. The quantum and transport mobilities increase rapidly with increasing total electron density, similar to a spin-degenerate 2DEG. Again, these mobilities depend strongly on the strength of the background impurity scattering although its concentration is relatively low. It should be noted that in principle, the Rashba parameter α should depend on sample parameters such as total electron density. Usually α increases with n_e because a larger n_e corresponds to a stronger inversion asymmetry of the confining potential. At relatively larger α and/or smaller n_e, the average transport mobility is mainly determined by electronic transitions occurring at the '−' spin branch because of the larger electron density there. Moreover, the numerical results presented here indicate that when $n_e \approx 10^{11} \sim 10^{12}\,\mathrm{cm}^{-2}$, the transport mobility $\mu_t \approx 10^4 \sim 10^5\,\mathrm{cm}^2/(\mathrm{V \cdot s})$ if $N_r \propto n_e$ and $N_b \ll N_r$ are taken into consideration. This is in line with experimental findings[1,7,8].

In the presence of a DC driving field, the electronic transition caused by impurity scattering in a spin split 2DEG has some unique features. When the SOI is present, the energy dispersion of a 2DEG is no longer parabolic (see Eq. (3) and Fig. 2) and the energy levels of different spin branches depend strongly on k (wavevector or momentum of an electron). In such a case, the spin orientation can change continuously with the momentum orientation when an electron moves in k-space. Thus, the SOI can shift ±branch of the spectrum continuously in k-space instead of a

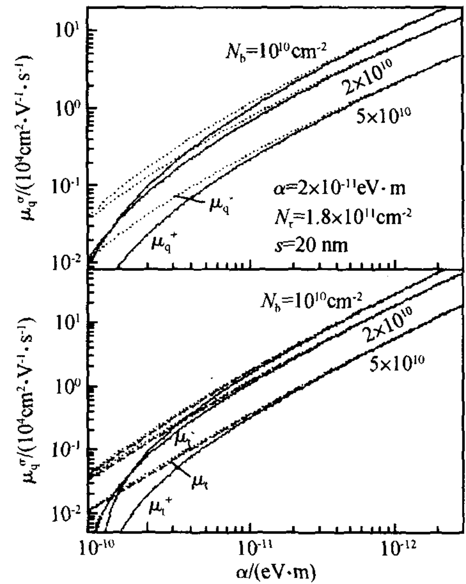

Fig. 11　Quantum and transport mobilities ($\mu_q^{\pm}$ and $\mu^{\pm}$ in the upper and lower panels) in different spin branches as a function of total electron density n_e at a fixed remote impurity concentration N_r for different background impurity concentrations N_b　Here, α is the Rashba parameter and s is the spacer distance.

quantized spectrum in energy space for the usual case. As a result, electrons are able to change their spin orientation simply through momentum exchange which can be more easily achieved than that through energy exchange for the usual case. These features are very favorable for separating transport mobilities μ^+ and μ^- determined by impurity scattering. However, an elastic and small-angle scattering in a 2DEG cannot change significantly the spin orientation of the conducting electrons, because it requires only a small momentum and energy exchange during a scattering event. On the basis that a quantum mobility measures the strength of the small-angle scattering, a small difference between μ_q^+ and μ_q^- can therefore be expected.

One important conclusion drawn from this theoretical study is that in spintronic systems such as InGaAs/InAlAs heterojunctions in which the SOI is mainly induced by the Rashba effect, small-angle scattering induced by electron-impurity interaction cannot alter significantly the spin orientation of the electrons. To achieve a large exchange of the spin orientation in different spin branches through electronic scattering in these

systems, inelastic and/or large-angle electronic transitions have to be involved. This result is useful in designing spintronic devices. It should be further noted that at present there is no simple experimental technique to measure the transport mobilities in different energy levels of electronic systems. However, recently developed ultrafast optoelectronic techniques, such as femtosecond pump-and-probe experiments, have been used to determine lifetimes (or mobilities) of electrons in different subbands in quantum-well structures[21]. Although the lifetimes obtained from ultrafast pump-and-probe experiments are not exactly the same as the transport lifetimes (mobilities) discussed in this paper, they are closely related and are of the same order of magnitude. Our results indicate that electronic transport lifetimes in different spin branches differ significantly at large Rashba parameters or small electron densities; this implies that they may be measured by femtosecond pump-and-probe experiments. We hope this will indeed be the case.

8 Concluding remarks

This study has developed a simple and tractable theoretical approach in dealing with spindependent electron distribution, electron-electron interaction, and quantum and transport mobilities in 2DEG systems in the presence of the spin-orbit interaction (SOI) induced by the Rashba effect. The important theoretical results obtained from this study are summarized as follows.

In the presence of SOI, the energy separation of the $\pm$spin branches is determined by the linear-in-k term. As a result, a stronger effect of the SOI on electron distribution, electron-electron screening and quantum and transport mobilities in different spin branches can be achieved in a system with a larger Rashba parameter and/or lower total electron density. The theoretical results have shown that over a wide range of sample parameters such as total electron density and Rashba parameter, the quantum mobilities for electrons in both $\pm$spin branches do not differ significantly, in line with experimental findings. This effect can be observed for electron interactions with remote and background impurities in an InGaAs/InAlAs heterojunction. The main reason behind this interesting and important phenomenon is that the spin-split electronic states and the SOI due to the Rashba effect depend strongly on the electron wavevector (or momentum). For elastic electron-impurity scattering, the quantum mobility is determined by an electronic transitions involving small-angle scattering or small momentum exchange. Thus, small-angle scattering induced by an electron-impurity interaction does not significantly change the spin transition of electrons in different spin branches. Consequently, the resulting quantum mobilities in different spin branches do not differ significantly.

Because transport mobility is determined by all possible electronic transition channels including large-angle scattering events, the contribution from the exchange of spin orientation in different spin branches, due to e. g., impurity scattering, can result in a rather significant difference in the transport mobilities in different spin branches. The theoretical results have shown that when $N_r \propto n_e$ and $N_r \gg N_b$ is taken into account, the obtained value of the average transport mobility is in line with the experimental data and the quantum and transport mobilities depend strongly on background impurity concentration N_b. We have found that the electron distribution, screening length and quantum and transport mobilities in different spin branches differ significantly for strong values of α. Recent experimental results have shown that in InAs- and InGaAs-based spintronic systems, the Rashba parameter can reach up to $\alpha \approx (3 \sim 4) \times 10^{11}$ eV·m[1,7]. Together with the fact that the strength of the SOI can be controlled by gates[8], we expect that the theoretical predictions in this paper will be tested in the near future.

Acknowledgements The author is a Research Fellow of the Australian Research Council. Discussions with P. Vasilopoulos (Concordia, Canada) and F. M. Peeters (Antwerp, Belgium) are gratefully acknowledged.

References

[1] Grundler D. Large Rashba splitting in InAs quantum wells due to electron wave function penetration into the barrier layers. Phys Rev Lett, 2000, 84: 6074

[2] Datta B, Das S. Electronic analog of the electro-optic mod-

ulator. Appl Phys Lett, 1990, 56: 665

[3] Koga T, Nitta J, Takayanagi H, et al. Spin-filter device based on the Rashba effect using a nonmagnetic resonant tunneling diode. Phys Rev Lett, 2002, 88: 126601

[4] Wang X F, Vasilopoulos P, Peeters F M. Spin-current modulation and square-wave transmission through periodically stubbed electron waveguides. Phys Rev B, 2002, 65: 165217

[5] SchÄapers Th, Engels G, Lange J, et al. Effect of the heterointerface on the spin splitting in modulation doped $In_xGa_{1-x}As/InP$ quantum wells for $B \to 0$. J Appl Phys, 1998, 83: 4324

[6] Rashba E I. Spin dynamics and spin transport. J Supercond: Incorporating Novel Magnetism, 2005, 18: 137

[7] Sato Y, Kita T, Gozu S, et al. Large spontaneous spin splitting in gate-controlled two-dimensional electron gases at normal $In_{0.75}Ga_{0.25}As/In_{0.75}Al_{0.25}As$ heterojunctions. J Appl Phys, 2001, 89: 8017

[8] Nitta J, Akazaki T, Takayanagi H. Gate control of spin-orbit interaction in an inverted $In_{0.53}Ga_{0.47}As/In_{0.52}Al_{0.48}As$ heterostructure. Phys Rev Lett, 1997, 78: 1335

[9] Schliemann J, Egues J C, Loss D. Variational study of the $\nu = 1$ quantum Hall ferromagnet in the presence of spin-orbit interaction. Phys Rev B, 2003, 67: 085302

[10] Luo J, Munekata H, Fang F F, et al. Effects of inversion asymmetry on electron energy band structures in GaSb/InAs/GaSb quantum wells. Phys Rev B, 1990, 41: 7685

[11] Tutuc E, De Poortere E P, Papadakis S J, et al. In-plane magnetic field-induced spin polarization and transition to insulating behavior in two-dimensional hole systems. Phys Rev Lett, 2001, 86: 2858

[12] Vitkalov S V, Sarachik M P, Klapwijk M P. Spin polarization of two-dimensional electrons determined from Shubnikovde Haas oscillations as a function of angle. Phys Rev B, 2001, 64: 73101

[13] Hai G Q, Studart N, Peeters F M, et al. Electron mobility in Si d-doped GaAs. Proceedings of the 22nd Int Conf on the Phys of Semicond, 1995: 823

[14] Koenraad P M, Heessels A C L, Blom F A P, et al. High-field transport in high carrier density $GaAs/Ga_{0.8}In_{0.2}As/Ga_{0.75}Al_{0.25}As$ heterostructures. Physica B, 1993, 184: 221

[15] Ando T, Fowler A B, Stern F. Electronic properties of two-dimensional systems. Rev Mod Phys, 1982, 54: 437

[16] Xu W. Plasmons of a two-dimensional electron gas in the presence of spin orbit interaction. Appl Phys Lett, 2003, 82: 724

[17] Xu W. Nonlinear optical absorption and LO-phonon emission in steady-state terahertz-driven three-dimensional electron gases. Phys Rev B, 1998, 57: 12939

[18] Xu W, Khmyrova I, Ryzhii V. Terahertz-photon-modified magnetotransport in a semiconductor in Voigt geometry. IBID B, 2001, 64: 85209

[19] Coleridge P T. Small-angle scattering in two-dimensional electron gases. Phys Rev B, 1991, 44: 3793

[20] Fletcher R, Zaremba E, D'Iorio M, et al. Persistent photoconduc- tivity and two-band effects in $GaAs/Al_xGa_{1-x}As$ heterojunctions. Phys Rev B, 1990, 41: 10649

[21] Sung C Y, Norris T B, Kushaa A A, et al. Femtosecond intersubband relaxation and population inversion in stepped quantum well. Appl Phys Lett, 1996, 68: 435